Interplay of Spinodal and Diffusion-Limited Aggregation in Formation of Nanocrystal Assembled 2D Islands

Yi-Ching Ou,[†] Konstantin S. Zhuravlev,[‡] Jiye Fang,[§] and Wen-Bin Jian*,[||]

Institute of Physics, NCTU, Hsinchu 30010, Taiwan, Institute of Semiconductor Physics, pr. Lavrentieva, 13, Novosibirsk 630090, Russia, Department of Chemistry, State University of New York at Binghamton, Binghamton, New York 13902-6000, United States, Department of Electrophysics, NCTU, Hsinchu 30010, Taiwan

Received: June 10, 2010; Revised Manuscript Received: September 14, 2010

Although self-organization of semiconductor nanocrystals (or quantum dots) into 3D superlattices and exploration of their collective optical, magnetic, and transport properties have been demonstrated, little is known about the underlying physics of self-assembly, growth mechanisms, and interdot-coupling-induced collective properties. Here we report a facile way of preparing nanocrystal-assembled 2D islands by drop-casting nanocrystal suspension on a hot substrate. Growth mechanisms such as scaling function, spinodal decomposition phase separation, and diffusion-limited aggregation are investigated based on the observation of quasi-monolayer coverage. After a curve fitting to several theoretical growth models, the pair bond (interaction) energy, critical nucleus size, and the phase of growth patterns were determined. Moreover, by heating the substrate and controlling the concentration of nanocrystal suspension, the spinodal decomposition and diffusion-limited aggregation can be tuned to modulate growth patterns of 2D nanocrystal islands. The interplay of these two mechanisms results in a variation of wavelength in spinodal growth patterns and of fractal pattern dimensions. By using this experimental approach, various sizes and shapes of nanocrystal-assembled 2D islands can be deposited on a flat surface of either graphite or gold.

Introduction

With the help of the top-down semiconductor technology, lithography, to reduce the lateral dimension of a 2D electron gas, the quantum dots (QDs) have been experimentally fabricated[1] to demonstrate their atomic-like physical properties, which have been introduced in theory for a long time.[2] Later on, a colloidal synthesis strategy[3] has been developed to fabricate QDs (or nanocrystals), which have been examined to show artificial atom features in optical properties,[4] magnetic properties due to orbital electrons,[5] and electronic structures.[6] Bearing a resemblance to atomic combination of forming a periodic crystal structure in a solid, these colloidal QDs are able to self-organize to form either 2D or 3D superlattices.[7−9] Thus, collective physical phenomena were proposed in theory and investigated in the QD-assembled superlattices. Recently, Ge and Brus illuminated that a system of 2D QD self-assembly can be suitably described by a 2D Lennard−Jones model, which may consist of two coexisting phases, resulting in a spinodal phase separation.[10] The same group (Brus's group) also demonstrated nucleation and growth behaviors,[11] and solvent-drying mediated self-assemblies of QDs at room temperature.[12] On the other hand, Jaeger's group reported their study aimed to a formation of long-range-ordered self-assembly[13] and a highly ordered QD monolayer.[14] More excitingly, binary nanocrystal superlattices,[15] coarsening,[16] and nanopatterning by molding[17] in QD formed superlattices have recently been conducted in experiments.

Theoretically, molecular-dynamic calculations of 2D Lennard−Jones model were applied to simulations of physisorbed systems, such as rare gases on graphite, to show interesting snapshots of island morphologies, particle trajectories, or growth patterns.[18,19] The fruitful phases of this 2D Lennard−Jones system illustrates various kinds of growth behaviors. These phases were commonly present on the reduced temperature and coverage (ρ^*, T^*) plane. Here, $\rho^* = \rho\sigma^2$ and $T^* = kT/\varepsilon$, where ρ is the particle density per unit area, σ is the hard-core diameter, k is the Boltzmann constant, T is the temperature, and ε is the pair bond energy (or the pair interaction energy). At a low coverage ($\rho^* \cong 10\%$), the critical nucleus size and the small cluster occurrences in thermal equilibrium can be learned and explored on the initial growth stage of a nucleation process.[20] In addition, the scaling function of the cluster size distribution[21,22] can be studied. With an increase of coverage, for example ρ^* up to ~40%, and at a temperature lower than the critical-point temperature of this system, a coexistence of liquid−gas or solid−gas phases should result in a spinodal decomposition of phase separation that could be obtained and recorded on microscopy images. The spinodal patterns have been discovered and observed in several systems such as quenched glass[23] and dried-up colloidal QDs[10−12] through a rapid cooling and a solvent drying processes, respectively. In these cases, it mainly focuses on diffusion-mediated motion and aggregation of the colloidal QDs.

On the other hand, in the case of colloidal QDs that are normally dispersed in a solvent, the solvent can play another important role in the growth and nucleation processes. The solvent is evaporated quickly when it is heated near its boiling point. Though the growth temperature is fixed at the boiling point, the rapid evaporation of the solvent shall lead to a reduction of the QD mobility on substrates, introducing an additional growth mechanism, diffusion-limited aggregation.[24] This effect could be enhanced especially when the QD assembly takes place on a substrate heated above the solvent boiling point.

* To whom correspondence should be addressed. E-mail: wbjian@mail.nctu.edu.tw.
[†] Institute of Physics, NCTU.
[‡] Institute of Semiconductor Physics.
[§] State University of New York at Binghamton.
[||] Department of Electrophysics, NCTU.

10.1021/jp105344b
Published on Web 09/29/2010

In previous reports,[10−12] the QD assembly was carried out at room temperature and the solvent was allowed to evaporate very slowly (up to one hour). The slow evaporation rate of the solvent drives a variation of the pair bond energy between QDs and a change of state from a high to a low reduced temperature. Unlike Brus's experiments,[10−12] we attempt to study the temperature effect on the (ρ^*, T^*) plane. By heating the substrate, the temperature dependence of growth behavior as well as the phase diagram of the colloidal QD system should exhibit. In this work, the solvent was evaporated rapidly (less than one minute) and the growth process can be quenched at such a high temperature. Thus, we can study the growth pattern at a fixed state, rather than transition states at different reduced temperatures. Other than an investigation on long-range ordered QD film, we concentrated our study on growth mechanisms of the spinodal decomposition and the diffusion-limited aggregation, and their application to syntheses of 2D QD islands. The QD-assembled 2D islands can be adopted as an approach to study collective properties in mesoscopic physics.

Experimental Section

PbSe QDs capped with oleic acid and triotylphosphine (TOP) were synthesized by using a high-temperature organic solution approach[3] and subsequently refined by using a size-selection procedure. Their crystalline structure and size distribution were investigated and described elsewhere.[25] The PbSe QDs can be stored by dispersing them in toluene. At least three drops of the QD suspension were put on a graphite substrate, which was heated on a hot plate above room temperature. PbSe QDs were deposited on the flat surface of highly oriented pyrolytic graphite (HOPG) substrates after a solvent evaporation. Raising the substrate temperature resulted in agitation of the QDs and varied the distribution of growth pattern coverage on a macroscopic scale. The resultant samples were subsequently studied using a field-emission scanning electron microscope (SEM, JEOL JSM-7000F). All SEM images were taken in a high vacuum at room temperature. The coverage of growth patterns was estimated based on the SEM images, and usually an area of $5 \times 5\ \mu m^2$ was selected for our studies. The coverage was calculated by using $\rho^* = \rho\sigma^2$, as described in the Introduction section. The windows of SEM imaging areas were varied on a millimeter scale, to broadly sample the coverage in QD growth patterns.

Results and Discussion

Colloidal PbSe QDs, consisting of a solid core of ~14.6 nm in diameter and a thin shell of organic molecules, were dispersed in toluene as solvent. Several drops of such a suspension were cast on graphite substrates that were preheated above room temperature. After the solvent was evaporated, the QDs formed 2D islands (clusters) with either ordered (solid phase) or disordered (fluid phase) arrangements. After a coverage variation of QD assembly on different places of the substrate, the 2D islands can be imaged using an SEM. Moreover, the difference in coverage and temperature lead to a change of island size and distribution on the growth patterns, and to an observation of various growth mechanisms. The reduced coverage was estimated from the ratio of the island area to the SEM image area and then multiplied by 0.9165.[11]

Growth Patterns and Phase Diagram. Various different growth patterns of QD islands on graphite surfaces are displayed in Figure 1. To understand and separate these growth patterns from each other, the following guidelines may be taken into account. The island number, island shape, island size distribution, and voids or holes on islands are important features to

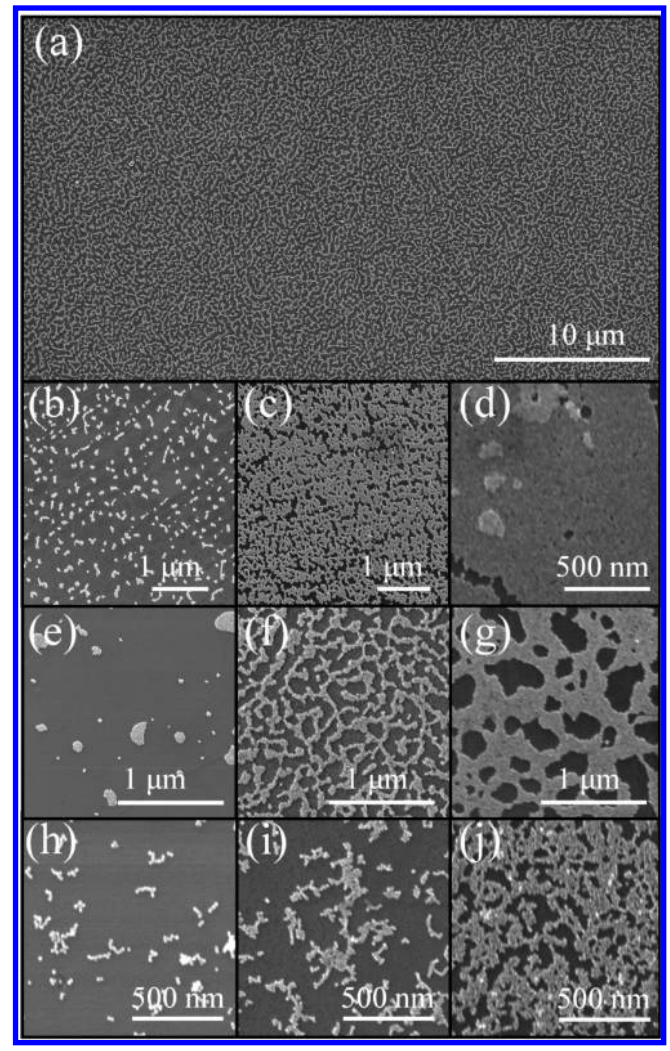

Figure 1. SEM images of PbSe QD patterns grown at substrate temperatures of 100 °C (a−d), 50 °C (e−g), and 180 °C (h−j). The QD coverage is a) 39%, b) 13%, c) 66%, d) 90%, e) 4%, f) 41%, g) 68%, h) 6%, i) 20%, and j) 61%.

categorize the growth patterns. There are several growth mechanisms including diffusion-mediated nucleation[18−23] and diffusion-limited aggregation[24] on the (ρ^*, T^*) plane. In the nucleation process of the growth, a large fluctuation in island size and a rounded, streamline island shape are important features. On the contrary, the diffusion-limited aggregation results in a growth pattern showing a comparatively uniform size and a dendritic, straight line in shape. In addition, gas, liquid, and solid phases and the spinodal phase decomposition process shall engage to modulate the final morphology of the growth pattern. The gas phase shall show a large number of tiny islands or a complementary pattern containing a large number of voids (smaller holes), whereas the solid phase will exhibit a large area of single islands with few holes and voids. The solid phase should further demonstrate an ordered lattice points on fast-Fourier-transformed images, in comparison with a ring structure existed in the liquid phase. Finally, the spinodal decomposition shall reveal a long-range order and a sinusoidal composition (QD area density) modulation.

Part a of Figure 1 shows an interconnected network, labyrinthine island pattern extending up to $40 \times 25\ \mu m^2$. The growth pattern with ~39% coverage was prepared at 100 °C. This pattern indicates undoubtedly a spinodal decomposition behavior scaling up to submillimeter that has never been

observed in a room-temperature QD assembly yet. Other growth patterns achieved at the same temperature with varied coverage of 13%, 66%, and 90% are presented in parts b−d of Figure 1. A complementary feature of small islands and voids illustrated in parts b and c of Figure 1 shows gas- and fluid-like phases, whereas a large island with few big holes, presented in part d of Figure 1, reveals a solid phase at a growth temperature as high as 100 °C.

When the substrate temperature was reduced to 50 °C, a nucleation behavior was observed in the island pattern change. Parts e, f, and g of Figure 1 illustrate a pattern variation with coverages of 4%, 41%, and 68%, respectively. An interconnected labyrinthine characteristic, signifying a spinodal decomposition behavior, can still be determined at such a low temperature (part f of Figure 1). Moreover, a complementary manner of islands and holes in parts e and g of Figure 1 demonstrate a nucleation process that unveils rounded islands or holes, and a large variation of island sizes implies a broadened island size distribution. Comparing part e of Figure 1 with part b of 1, it can evidently be detected that a considerably large number of small islands with a uniform size appear in part b of Figure 1, whereas several area-unequal islands with a rounded shape show up in part e of Figure 1, although the coverage in both cases are of the same order. As a result, the gas phase and the nucleation growth behavior can definitely be differentiated from each other. Furthermore, as the *substrate temperature* was raised much higher than the boiling point of the solvent, the diffusion length of the QDs becomes shorter which in turn makes a transition from diffusion-mediated to diffusion-limited growth or aggregation. The shorter diffusion length mainly comes from a shorter time of solvent evaporation. As shown in parts h−j of Figure 1, the growth patterns were formed at a substrate temperature of 180 °C with different coverage areas of 6%, 20%, and 61%. The substrate temperature indicates that the growth temperature shall be no lower than the boiling point of toluene, whereas the elevated substrate temperature must cause rapid evaporation of the solvent, resulting in a diffusion-limited growth behavior. Unlike the gas phase and the nucleation growth patterns, part h of Figure 1 demonstrates a few of straight, chainlike islands, showing that an increase of the coverage results in a formation of chain-like islands or dendritic islands. Further increase of the coverage (refer to part j of Figure 1) shows a dendritic islands as dominant structure and a shape of straight line on the edge of islands. To compare with those prepared at 100 and 50 °C (parts d and g of Figure 1), the growth pattern in part j of Figure 1 reveals a thin strip rather than rounded holes.

Unlike the growth at room temperature that a drying process could induce an increase of pair bond energy ε (a decrease of reduced temperature) and change the state from a high to a low reduced temperature,[10,11] the high temperature growth causes a rapid evaporation of the solvent so that the resultant patterns could be quenched. To put all growth patterns (Figure 1) on the (ρ^*, T^*) plane, we need to determine the pair bond energy. Here, the island number variation as a function of coverage at various temperatures (part a of Figure 2) for the same image size of 5×5 μm^2 is used to determine the pair bond energy, which can be verified further in another analysis in the following paragraphs. We found that the growth pattern at 50 °C reveals the lowest island density and a decrease of island density from $\sim$100 to $\sim$10 μm^{-2} as the coverage is raised from 10% to 40%. This low island density is mainly due to the nucleation growth and the spinodal decomposition behaviors. As shown in parts e−g of Figure 1, islands can be counted individually only when

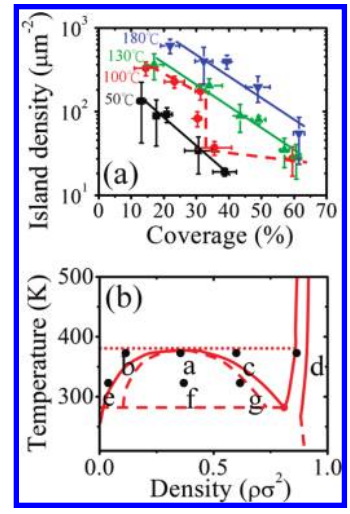

Figure 2. a) Island density as a function of QD coverage grown at various different temperatures indicated on graph. The SEM images with a coverage of higher than 10% are used in this analysis. Error bars of data points are presented as well. The solid and dashed lines are only guides to eyes. b) phase diagram of a 2D Lennard−Jones system, reproduced from refs 18 and 11. The symbols, a−g, point to the growth conditions of the patterns shown in Figure 1. The dotted line indicates the boiling point (110.6 °C) of the toluene solvent.

a coverage is much lower than $\sim$50%. With higher coverage, the spinodal decomposition process drives the islands to coalesce into one or few large islands. With much higher coverage, the nucleation mechanism turns on again and we can observe many large holes in a single, large island in part g of Figure 1. Conversely, when the coverage is about 10−20% and the temperature is increased up to 100 °C (Figure 2), the island density is doubled or tripled in number, probably owing to a transition from the state in nucleation region to a gas (fluid) state on the phase diagram. The island density increases further but not so much when the substrate temperature is of 130 or 180 °C. Again, the growth temperature is around the boiling point of toluene and the elevated substrate temperature only causes toluene to evaporate quickly and induces diffusion-limited aggregation. It was observed that the island density decreases exponentially with coverage at almost all temperatures, whereas it shows a steepest descent with a coverage of $\sim$35% for the growth at 100 °C. This great deal of island density variation is attributed to a phase transition from the gas phase, featured a large island density, to the states in spinodal decomposition regime, revealing few coalesced islands and low island density. It is noted that the data at 50 °C probably reveal a state variation on the phase diagram from the nucleation to the spinodal decomposition regime. States on both of those two regions share the same feature of a small amount of islands. Moreover, the data at 130 and 180 °C imply a phase transition from the gas to the liquid phases, sharing the same feature of a larger amount of islands. Through this island density analysis, we conjecture that the temperature of 100 °C shall be very close to the critical-point temperature of this 2D QD system. We therefore propose a reduced temperature T^* of 0.54[18] (slightly lower than the critical-point temperature, $T^* = 0.55$) to be at 100 °C then the pair bond energy ε of $690k \cong 59$ meV can be estimated.

After the pair bond energy is determined, those states of growth patterns (Figure 1) can be assigned and marked on the 2D Lennard−Jones phase diagram of part b of Figure 2. On this phase diagram, the top point of solid curve near the symbol **a** is close to the gas−liquid critical-point temperature ($T^* =$

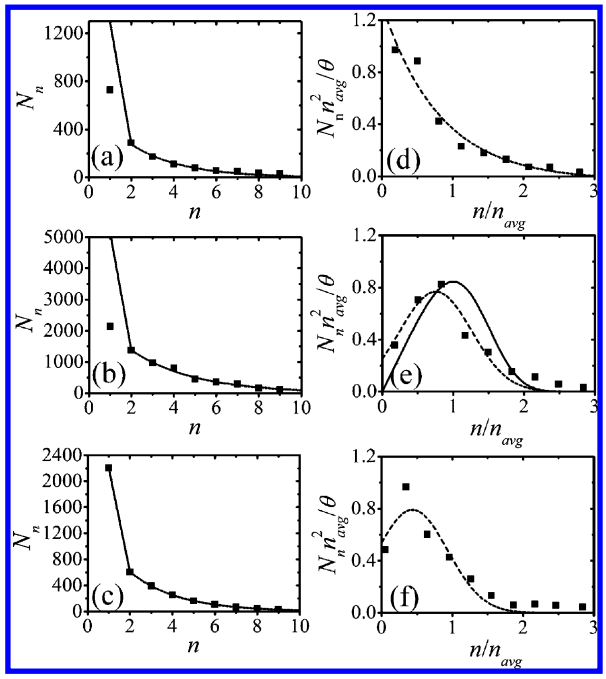

Figure 3. Occurrence as a function of aggregation number (n, number of QDs) corresponding to small islands with 3−9 QDs at a) 50, b) 100, and c) 180 °C. The solid lines present the fitting results. Scaled island size distributions at d) 70, e) 100, and f) 130 °C. The coverage are d) 4, e) 13, and f) 16%. The dashed lines are guides to eyes. The solid line in Figure (e) represents the scaling function corresponding to a critical nucleus size $n = 1$ and a stable cluster size $n \geq 2$.

0.55)[18] and the dashed line indicates the triple-point temperature ($T^* = 0.41$).[18] The area between solid and dashed curves belongs to a nucleation growth process and the area under the dashed curve and the dashed line belongs to a spinodal decomposition region. The identification of states on the phase diagram gives reasonable explanation of growth patterns shown in parts a−g of Figure 1. As pointed out, only the substrate temperature of the growth patterns shown in parts h−j of Figure 1 is specified, so their states are not presented in part b of Figure 2. A dotted line indicates the boiling point of toluene solvent to emphasize that the diffusion-limited aggregation shall be enhanced at a substrate temperature above this line.

Growth Mechanisms. Several growth mechanisms play important roles to modulate the growth pattern. In the initial growth stage, the cluster occurrence correlates with a decrease of free energy in cluster formation. Moreover, the scaling function can be used to evaluate the critical nucleus size. As the coverage increases, a growth mechanism of the spinodal decomposition is involved. Moreover, as for our case of the QD growth in solution, a higher substrate temperature and the rapid evaporation of solvent shall induce a diffusion-limited aggregation.

Parts a−c of Figure 3 show the occurrence N of small clusters as a function of the cluster aggregation number n, calculated on the basis of fifty SEM images with an area of 2.8 × 2.1 μm^2. The occurrence of single QD, 2-QD, 3-QD, and n-QD clusters are denoted as N_1, N_2, N_3, and N_n, respectively. The data present with n in a range from 3 to 9. Because the formation of n-QD cluster from isolated QDs makes a decrease of energy ($-E_n$) and affects the occurrence (possible configurations) through a thermal equilibrium process, the occurrence shall follow the form[20]

$$N_n = N_0(N_1/N_0)^n \exp(E_n/kT) \quad (1)$$

where N_0 is the total number of QDs to cover the whole area of the SEM image. Using the same assumption in ref 11, each bond causes a decrease of free energy (αkT) and the formation of n-QD cluster for $n > 1$ leads to a lowering of free energy ($E_n = (2n - 3)\alpha kT$). This gives

$$N_n = N_0(N_1/N_0)^n \exp((2n - 3)\alpha) \quad (2)$$

Usually the occurrence of a single QD is not easy to be counted possibly due to the limit of the image resolution. The other reason could be attributed to the fact that the stable nucleus size is larger than one, and therefore a single QD has a high tendency to coalesce on big islands. A nonlinear least-squares fitting was used to evaluate N_1 and α. The fitting results are displayed as solid curves in parts a−c of Figure 3. It is noted that eq 2 is valid only for $n \geq 2$. A straight line is therefore given to simply connect the two calculated values of N_1 and N_2. The parameter α was determined to be 1.13, 0.99, and 0.85 for growth data at 50, 100, and 180 °C, respectively. Thus the pair bond energies (αkT) were estimated to be 31, 32, and 33 meV for clusters grown at 50, 100, and 180 °C. This gives an average value of about 32 meV, which is about one-half of the pair bond energy $\varepsilon \cong 59$ meV estimated from part a of Figure 2. In particular, the pair bond energy is very close to the calculated attraction energy of 40 meV (1.6 kT) and experimentally evaluated value of 88 meV (3.5 kT), as reported in ref 11.

On the other hand, the critical nucleus size can be determined by a scaled island size distribution. The island size distribution, which is normally N_n as a function of the QD number n, is scaled to $N_n n^2_{avg}/\theta$ as a function of n/n_{avg}, where θ is the coverage and n_{avg} is the average size of the QD-formed islands. The scaled island size distributions with specified coverage of 5−15% and at different temperatures are displayed in parts d−f of Figure 3. Because it is analyzed at low coverage, we can ignore the spinodal decomposition behavior. Thus only the temperature and solvent drying effects will be taken into account. In part e of Figure 3, a solid line of scaling function is displayed to indicate a critical nucleus of one QD, which means that island size with two more QDs are stable. Part d of Figure 3 shows that, at 70 °C, even a single QD can be stable and exist on the graphite surface. At a higher temperature of 100 °C (part e of Figure 3), the excess thermal energy makes single QD more mobile and islands having at least two QDs can stably exist in growth patterns. The critical nucleus size therefore increases and the smallest stable island must consist of at least two QDs. This result is in line with the temperature effect on critical nucleus reported for atomic growth behavior.[26] The critical nucleus size slightly changes back to one QD at an elevated temperature, 130 °C (part f of Figure 3). We believe that, at this high temperature, the solvent drying process should be taken into account. More interestingly, part e of Figure 3 indicates a stable cluster of $n \geq 2$. This result can also be confirmed in the bonding energy analysis displayed in part b of Figure 3. We found that the experimental value is much lower than the calculated value of occurrence of single adsorbed QD for growth at 100 °C. On the contrary, the measured occurrence of single QD is more close to the calculated value in parts a and c of Figure 3. It is noticed that the growth behavior varies with a different substrate temperature above the solvent boiling point (parts c and f of Figure 3).

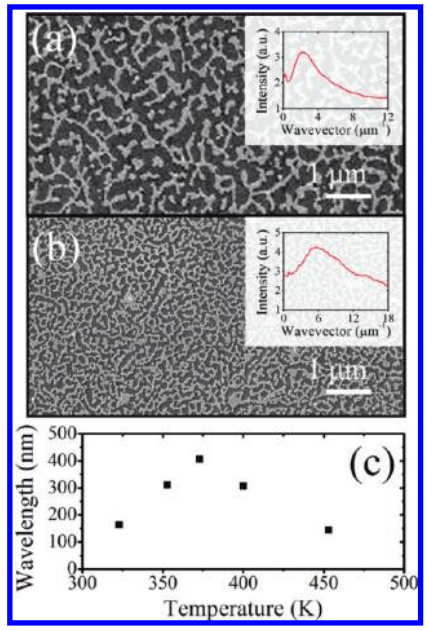

Figure 4. a) SEM image of a spinodal pattern grown with coverage of ~38% at 100 °C. b) SEM image of a spinodal pattern grown with coverage of 45% at 50 °C. The insets show fast-Fourier-transformed and radial averaged intensity as a function of inverse wavelength. c) Wavelength at maximum intensity, estimated from the intensity distribution, like the inserts of parts (a) and (b), for QD growth with coverage of ~42% and at different temperatures.

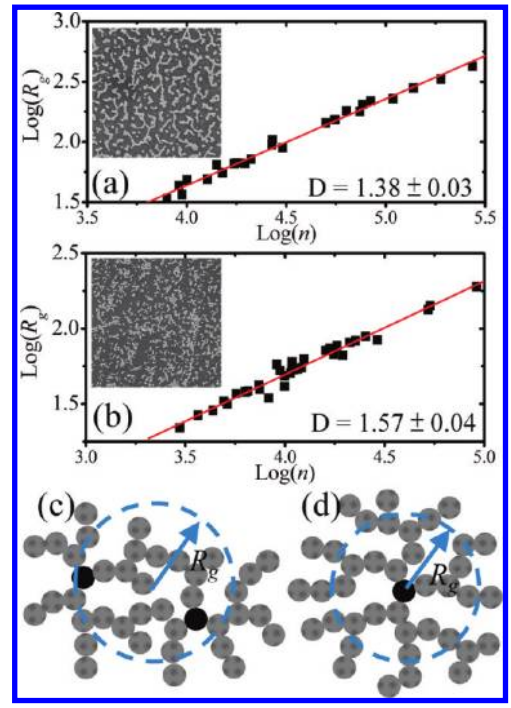

Figure 5. Gyration radius, R_g, has a power law dependence on the aggregation number, n, in double logarithm scales for QD growth at a) 100 °C and b) 180 °C with coverage of 21% and 18%, respectively. Corresponding SEM images are displayed in the insets. Schemes of c) cluster diffusion and d) single-particle diffusion models.

With an increase of coverage, owing to a coexistence of two phases, the growth mechanism of spinodal decomposition engages to modulate sinusoidally the compositional (QD density) variation that generates a macroscopically uniform island size distribution with an interconnection labyrinthine structure. Two spinodal growth patterns assembled at 100 and 50 °C are exhibited in parts a and b of Figure 4, respectively. Evidently, different wavelengths of the sinusoidal compositional modulation can be identified between the two SEM images. This wavelength variation has not been experimentally discovered in room-temperature QD assembly yet.[10−12] According to the spinodal phase separation theory,[23] the wavelength is inversely proportional to the square root of the undercooling temperature, $\lambda \propto (T_C - T)^{-1/2}$, where T_C is the critical-point temperature. To evaluate the wavelength of the sinusoidal composition modulation, the radial average intensity of fast-Fourier-transformed image was calculated (inserts of Figure 4 as examples). The wavelengths at maximum intensity are 450 and 176 nm for growth patterns shown in parts a and b of Figure 4, respectively. The temperature behavior of the wavelength at maximum intensity is thus summarized in part c of Figure 4. When the temperature is increased above room temperature, it was found that the wavelength increases up to a maximum value at 100 °C. More excitingly, the spinodal growth patterns remain observable even if the substrate temperature is much higher than the critical-point temperature. This result is in contradiction to the gas or fluid phase above critical-point temperature that is predicted in the phase diagram (part b of Figure 2). In addition, the wavelength at maximum intensity shown in part c of Figure 4 reveals a decline with an increase of the substrate temperature above the toluene boiling point. We therefore conclude that the elevated substrate temperature makes the solvent to evaporate and the growth mechanism of diffusion-limited aggregation is in turn employed to modify the growth pattern. Because of the rapid evaporation of toluene solvent, the decrease of wavelength at elevated temperature shall be resulted from a reduced evolution time[27] required for long-wavelength spinodal patterns such as that displayed in part a of Figure 4. The interplay between spinodal decomposition and diffusion-limited aggregation could be studied and further controlled by using substrate temperature and QD coverage (concentration of QD suspension) so as to grow 2D islands with specified sizes and shapes.

Because the solvent evaporation introduces a diffusion-limited growth mechanism, the analysis method used in atomic growth of diffusion-limited aggregation can certainly be implemented here. Either the density−density correlation function or the radius of gyration as a function of cluster size (aggregation number n)[24] can be applied to the investigation into the randomly aggregated fractal structure. The analysis using radius of gyration, R_g, which is a mean square distance between the particle and the center of mass of the cluster, is adopted in this study. A fractal dimension D is introduced in the expression[24]

$$n \sim R_g^D \tag{3}$$

Log−log plots of R_g as a function of aggregation number n are given in parts a and b of Figure 5 for patterns (the inserts) grown at 100 and 180 °C respectively, with coverage of ~20%. The fractal dimensions D's are estimated to be 1.38 and 1.57 as indicated in the figure. This observable difference in D shall be originated from the substrate temperature. At the temperature of 100 °C and below the toluene boiling point, the toluene solvent shall not be evaporated so quickly and the as-aggregated clusters may diffuse on surface and coalesce into larger ones. This experimental result of fractal dimension $D \cong 1.38$ is considerably close to the cluster diffusion models given by P. Meakin[28] ($D \cong 1.47$) and M. Kolb et al.[29] ($D \cong 1.38$). On the other hand, a high substrate temperature of 180 °C leads to a random aggregate of cluster which by no means can diffuse on substrate anymore due to the solvent dry-up. This result of fractal

dimension $D \cong 1.57$ is in line with the predicted value of 1.67 using the WS model.[24] The cluster diffusion at 100 °C seems to be in connection with a long evolution time required to produce a long wavelength of spinodal growth patterns as discussed above. Here, the interplay between the spinodal decomposition and the diffusion-limited aggregation appears again. Two schemes to illustrate the cluster diffusion and single-particle diffusion models are given in parts c and d of Figure 5. For the same aggregation number n, the cluster diffusion causes a longer radius of gyration and thus a smaller fractal dimension.

Conclusions

Various kinds of 2D growth patterns have been prepared through a facile way of dropping toluene-dissolved PbSe QD suspension on a hot graphite substrate. These growth patterns have been extensively analyzed, and related phase diagram, pair bond energy, and growth mechanisms have accordingly been studied. The pair bond energy, $\varepsilon \cong 59$ meV, between PbSe QDs is derived from a simple analysis of substrate temperature and coverage dependences of island density. This determines the states of growth patterns on 2D Lennard−Jones phase diagram. Another analysis on occurrences of small clusters in thermal equilibrium gives a pair bond energy of ∼32 meV during cluster formation. Moreover, with a low coverage, a scaled function of island size distribution was used to determine the critical nucleus size of either 0 or 1 for this system. With high coverage, the spinodal decomposition induced compositional modulation was investigated and the sinusoidal wavelength as a function of temperature is summarized. This outcome indicates a decrease of the wavelength in spinodal patterns due to both the undercooling temperature below the critical-point temperature and the restricted evolution time for pattern formation. In addition, the elevated substrate temperature introduces a diffusion-limited growth mechanism. Through a comparison of patterns at different temperatures, the diffusion-limited aggregation reveals cluster and single-particle diffusions at temperatures of near and above, respectively, the solvent boiling point. The interplay between spinoal decomposition and diffusion-limited aggregation is under control by using substrate temperature so as to make 2D PbSe QD islands on a flat graphite surface.

Acknowledgment. This work was supported by the Taiwan National Science Council under Grant Numbers NSC 98-2112-M-009-013-MY2 and NSC 98-2923-M-009-001-MY2, and by the MOE ATU Program. J.F. thanks US NSF support (DMR-0731382).

References and Notes

(1) Hansen, W.; Smith, T. W.; Lee, K. Y.; Brum, J. A.; Knoedler, C. M.; Hong, J. M.; Kern, D. P. Zeeman Bifurcation of Quantum-Dot Spectra. *Phys. Rev. Lett.* **1989**, *62*, 2168–2171.

(2) Reimann, S. M.; Manninen, M. Electronic Structure of Quantum Dots. *Rev. Mod. Phys.* **2002**, *74*, 1283–1342.

(3) Murry, C. B.; Sun, S.; Gaschler, W.; Doyle, H.; Betley, T. A.; Kagan, C. R. Colloidal Synthesis of Nanocrystals and Nanocrystal Superlattices. *IBM J. Res. Dev.* **2001**, *45*, 47–55.

(4) Alivisatos, A. P. Semiconductor Clusters, Nanocrystals, and Quantum Dots. *Science* **1996**, *271*, 933–937.

(5) Jian, W. B.; Lu, W.; Fang, J.; Chiang, S. J.; Lan, M. D.; Wu, C. Y.; Wu, Z. Y.; Chen, F. R.; Kai, J. J. Orbital Susceptibilities of PbSe Quantum Dots. *J. Chem. Phys.* **2006**, *124*, 064711/1−4.

(6) Banin, U.; Cao, Y.; Katz, D.; Millo, O. Identification of Atomic-Like Electronic States in Indium Arsenide Nanocrystal Quantum Dots. *Nature* **1999**, *400*, 542–544.

(7) Murray, C. B.; Kagan, C. R.; Bawendi, M. G. Self-Organization of CdSe Nanocrystallites into Three-Dimensional Quantum Dot Superlattices. *Science* **1995**, *270*, 1335–1338.

(8) Motte, L.; Billoudet, F.; Pileni, M. P. Self-Assembled Monolayer of Nanosized Particles Differing by Their Sizes. *J. Phys. Chem.* **1995**, *99*, 16425–16429.

(9) Wang, Z. L. Structure Analysis of Self-Assembling Nanocrystal Superlattices. *Adv. Mater.* **1998**, *10*, 13–30.

(10) Ge, G.; Brus, L. Evidence for Spinodal Phase Separation in Two-Dimensional Nanocrystal Self-Assembly. *J. Phys. Chem. B* **2000**, *104*, 9573–9575.

(11) Tang, J.; Ge, G.; Brus, L. E. Gas-Liquid-Solid Phase Transition Model for Two-Dimensional Nanocrystal Self-Assembly on Graphite. *J. Phys. Chem. B* **2002**, *106*, 5653–5658.

(12) Rabani, E.; Reichman, D. R.; Geissler, P. L.; Brus, L. E. Drying-mediated Self-Assembly of Nanoparticles. *Nature* **2003**, *426*, 271–274.

(13) Lin, X. M.; Jaeger, H. M.; Sorensen, C. M.; Klabunde, K. J. Formation of Long-Range-Ordered Nanocrystal Superlattices on Silicon Nitride Substrates. *J. Phys. Chem. B* **2001**, *105*, 3353–3357.

(14) Bigioni, T. P.; Lin, X. M.; Nguyen, T. T.; Corwin, E. I.; Witten, T. A.; Jaeger, H. M. Kinetically Driven Self Assembly of Highly Ordered Nanoparticle Monolayers. *Nat. Mater.* **2006**, *5*, 265–270.

(15) Urban, J. J.; Talapin, D. V.; Shevchenko, E. V.; Kagan, C. R.; Murray, C. B. Synergism in Binary Nanocrystal Superlattices Leads to Enhanced P-Type Conductivity in Self-Assembled PbTe/Ag_2Te Thin Films. *Nat. Mater.* **2007**, *6*, 115–121.

(16) Blunt, M. O.; Martin, C. P.; Ahola-Tuomi, M.; Pauliac-Vaujour, E.; Sharp, P.; Nativo, P.; Brust, M.; Moriarty, P. J. Coerced Mechanical Coarsening of Nanoparticle Assemblies. *Nat. Nanotechnol.* **2007**, *2*, 167–170.

(17) Cheng, W.; Park, N.; Walter, M. T.; Hartman, M. R.; Luo, D. Nanopatterning Self-Assembled Nanoparticle Superlattices by Moulding Microdroplets. *Nat. Nanotechnol.* **2008**, *3*, 682–690.

(18) Barker, J. A.; Henderson, D.; Abraham, F. F. Phase Diagram of the Two-Dimensional Lennard-Jones System; Evidence for First-Order Transitions. *Physica* **1981**, *106A*, 226–238.

(19) Toxvaerd, S. Phase Transitions in a Two-Dimensional System. *Phys. Rev. Lett.* **1980**, *44*, 1002–1004.

(20) Walton, D. Nucleation of Vapor Deposits. *J. Chem. Phys.* **1962**, *37*, 2182–2188.

(21) Bartelt, M. C.; Evans, J. W. Scaling Analysis of Diffusion-Mediated Island Growth in Surface Adsorption Processes. *Phys. Rev. B* **1992**, *46*, 12675–12687.

(22) Amar, J. G.; Family, F. Critical Cluster Size: Island Morphology and Size Distribution in Submonolayer Epitaxial Growth. *Phys. Rev. Lett.* **1995**, *74*, 2066–2069.

(23) Cahn, J. W. Phase Separation by Spinodal Decomposition in Isotropic Systems. *J. Chem. Phys.* **1965**, *42*, 93–99.

(24) Witten, T. A.; Sander, L. M. Diffusion-Limited Aggregation, a Kinetic Critical Phenomenon. *Phys. Rev. Lett.* **1981**, *47*, 1400–1403.

(25) Ou, Y. C.; Wu, J. J.; Fang, J.; Jian, W. B. Probing Capacitive Coupling and Collective Transport in PbSe Quantum-Dot Arrays Using Scanning Tunneling Spectroscopy. *J. Phys. Chem. C* **2009**, *113*, 7887–7891.

(26) Stroscio, J. A.; Pierce, D. T. Scaling of Diffusion-Mediated Island Growth in Iron-on-Iron Homoepitaxy. *Phys. Rev. B* **1994**, *49*, 8522–8525.

(27) Sofonea, V.; Mecke, K. R. Morphological Characterization of Spinodal Decomposition Kinetics. *Eur. Phys. J. B* **1999**, *8*, 99–112.

(28) Meakin, P. Formation of Fractal Clusters and Networks by Irreversible Diffusion-Limited Aggregation. *Phys. Rev. Lett.* **1983**, *51*, 1119–1122.

(29) Kolb, M.; Botet, R.; Jullien, R. Scaling of Kinetically Growing Clusters. *Phys. Rev. Lett.* **1983**, *51*, 1123–1126.

JP105344B